

Supercooling and fragile glassiness in a dipolar kagome Ising magnet

James Hamp,^{1,*} Roderich Moessner,² and Claudio Castellano¹

¹*TCM Group, Cavendish Laboratory, University of Cambridge,
J. J. Thomson Avenue, Cambridge CB3 0HE, United Kingdom*

²*Max-Planck-Institut für Physik komplexer Systeme, Nöthnitzer Straße 38, Dresden 01187, Germany*

(Dated: June 8, 2018)

We study equilibration and ordering in the classical dipolar kagome Ising antiferromagnet, which we show behaves as a disorder-free fragile spin glass. By identifying an appropriate order parameter, we demonstrate a transition to the ordered state proposed by Chioar *et al.* [Phys. Rev. B **93**, 214410 (2016)] with a 12-site unit cell that breaks time-reversal and sublattice symmetries, and further provide evidence that the nature of the transition is first order. Upon approaching the transition, the spin dynamics slow dramatically. The system readily falls out of equilibrium, overshooting the transition and entering a supercooled liquid regime. Using extensive Monte Carlo simulations, we show that the system exhibits super-Arrhenius behaviour above the ordering transition. The relaxation time diverges according to a Vogel-Fulcher form at a finite ‘glass transition’ temperature in the supercooled regime. Such behaviour, characteristic of fragile glasses, is particularly remarkable as the model is free of quenched disorder, does not straightforwardly conform to the avoided criticality paradigm, and is simple and eminently realisable in engineered nanomagnetic arrays.

I. INTRODUCTION

It is well-known that the presence of disorder in a system can generate a rugged free energy landscape resulting in slow or glassy dynamics. The converse – the appearance of glassiness in the absence of disorder – is far less understood. Due to their complex energy landscapes exhibiting multiple minima, geometrically frustrated systems with long-range interactions are natural candidates in this regard^{1,2}.

In recent years, interesting slow dynamics in the absence of disorder has been uncovered in electronic Coulomb liquids on the triangular lattice at quarter-filling³. The dynamics of electrons on the frustrated kagome lattice has also received some attention of late⁴, but strong metastability effects mean there remain open questions about the nature of the ground state in that system.

Slow dynamics persist even for faster-decaying interactions (dipolar instead of Coulomb), in systems without particle-number conservation, i.e., spin systems. This was demonstrated for instance in Ref. 5, where due to strong freezing and metastability effects the nature of the ground state could not be convincingly established.

In this paper, we explore in greater detail the latter case, namely that of frustrated Ising spins on the kagome lattice subject to dipolar interactions – the dipolar kagome Ising antiferromagnet (DKIAFM). We begin by identifying an order parameter for the state proposed by Chioar *et al.*⁵ This allows us to confirm the nature of the ground state in extensive simulations of small systems, and to provide evidence that the transition is first order. Upon approaching the transition, the spin dynamics slow dramatically and a supercooled liquid regime appears. Despite the propensity of the system to fall out of equilibrium, we are able to reach thermodynamic equilibrium in Monte Carlo simulations for systems of up to ~ 300 spins. At equilibrium above the ordering transition

we find robust evidence of super-Arrhenius behaviour. The relaxation time τ appears to diverge according to a Vogel-Fulcher law, $\tau \sim \exp[\Delta/(T - T_0)]$, characteristic of fragile glasses, at a temperature smaller than the thermodynamic transition temperature. We provide some evidence that the slowing down is due to the existence of many low-lying metastable states exhibiting dendritic stripes of emergent charges.

Our results highlight the dipolar kagome Ising antiferromagnet (DKIAFM) as particularly suitable for the study of disorder-free glassy dynamics. On the one hand, fragile glass behaviour, where the timescale diverges at a finite temperature in the supercooled liquid regime, is hard to come by in non-disordered systems in two dimensions⁶. On the other hand, theoretical models of glasses without disorder where the thermodynamic behaviour is well understood are typically limited to the rather artificial multi-spin Hamiltonians of kinetically constrained models⁷, difficult to realise in a laboratory, and unlikely to occur in real materials. The DKIAFM exhibits the above interesting features with a Hamiltonian that is eminently realistic.

The behaviour exhibited by the DKIAFM may be relevant to monolayer colloidal crystals^{8,9} where recent advances have enabled the study of slow dynamics of frustrated systems in real time. It is also relevant to artificial nanomagnetic arrays, where lattices can be engineered and studied in real time at a ‘microscopic’ scale¹⁰. Another potential avenue where this model could be realised in experiments is that of cold polar molecules¹¹ and atomic gases with large magnetic dipole moments¹². Of particular interest there would be the possibility of investigating how the relaxation time scales and glassy behaviour may be affected by quantum dynamics. Finally, (layered) kagome spin lattices occur in solid state materials, and can be combined with the crystal field physics of rare earth ions to achieve the desired easy-axis (Ising) nature and leading dipolar interactions^{13–15}.

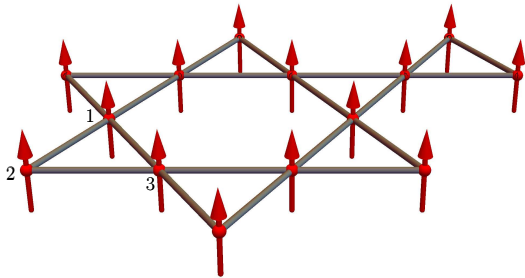


FIG. 1. The dipolar kagome Ising antiferromagnet. The spins \mathbf{S}_i (red arrows) share a global Ising easy-axis perpendicular to the plane (in the $\hat{\mathbf{e}}_z$ direction) and interact via nearest-neighbour exchange interactions of strength J , and long-range dipolar interactions of characteristic strength D . The sublattices $a = \{1, 2, 3\}$ are numbered.

The remainder of the paper is organised as follows. In Sec. II we introduce the dipolar kagome Ising antiferromagnet (DKIAFM) model. In Sec. III we discuss the ordering displayed by the model and the nature of the transition to the ground state. In Sec. IV we discuss the dynamic properties of the model at low temperatures, in particular the spin relaxation. In Sec. V we discuss the dynamics of the model out of equilibrium. Finally in Sec. VI we conclude and discuss the connection to experiments.

II. MODEL

We consider the dipolar kagome Ising antiferromagnet⁵ (illustrated in Fig. 1), in which N classical spins \mathbf{S}_i are arranged on the kagome lattice and share a global Ising easy-axis perpendicular to the plane (in the $\hat{\mathbf{e}}_z$ direction). As such, the spins $\mathbf{S}_i = \mu\sigma_i\hat{\mathbf{e}}_z$ can be described by the Ising pseudospin variables $\{\sigma_i = \pm 1\}$, and μ is the magnitude of the spin magnetic moment (we set $\mu = 1$ where relevant in the remainder of the paper).

The Hamiltonian comprises an exchange term of strength J between spins at nearest neighbour lattice sites $\langle ij \rangle$, and long range dipolar interactions of characteristic strength $D = (\mu_0/4\pi)\mu^2/r_{\text{nn}}^3$ between all pairs of spins, where r_{nn} is the nearest-neighbour distance of the lattice. The Hamiltonian is given by

$$\mathcal{H} = -J \sum_{\langle ij \rangle} \sigma_i \sigma_j + D r_{\text{nn}}^3 \sum_{j>i} \frac{\sigma_i \sigma_j}{|\mathbf{r}_{ij}|^3}, \quad (1)$$

where $\mathbf{r}_{ij} \equiv \mathbf{r}_j - \mathbf{r}_i$ is the separation between spins at lattice sites i and j . The Hamiltonian (1) is equivalent to dipolar spin ice on the kagome lattice (see e.g., Ref. 16) in the limit of spins rotated so that they are perpendicular to the plane.

We are interested here in the case where both interactions are antiferromagnetic, namely $J < 0$ and $D > 0$.

The case where $D = 0$ is known to be fully frustrated and does not order down to zero temperature¹⁷. The phase diagram of the case where $J = 0$ is less well understood but the system is again strongly frustrated, with any ordering (if present at all) suppressed down to temperatures $T \ll D$ ¹⁸. A more detailed discussion of the frustration in Eq. (1) is given in Appendix A.

Throughout the remainder of this paper we consider the coupling parameters from Ref. 5, namely $D = 1$ K and $J = -0.5$ K (in the remainder of the paper we set $k_B = 1$ and measure all energies in Kelvin).

III. ORDER PARAMETER AND NATURE OF THE TRANSITION

Long-range ordering has not yet been directly observed in the DKIAFM. In Ref. 5 it was found that at very low temperatures the system exhibits freezing of single spin-flip and loop dynamics whilst seemingly being on the verge of an ordering transition, as evidenced by the onset of a pronounced peak in the heat capacity. A candidate for the ground state of the present model was proposed and shown to be consistent with the available thermodynamic data from simulations. The state, illustrated in Fig. 2, has a 12-site magnetic unit cell that can be visualised as arising from tessellating trapezoids of alternating spins to form 7 shapes. For more details on this construction see Ref. 5; in the following we refer to this state as the proposed ground state.

The state is sixfold degenerate – under threefold rotation (sublattice) symmetry and twofold time-reversal symmetry. Upon assigning an emergent charge variable to each of the up- and down-type triangles (Δ and ∇) on the kagome lattice,

$$Q_{\Delta} = \sum_{i \in \Delta} \sigma_i; \quad (2)$$

$$Q_{\nabla} = - \sum_{i \in \nabla} \sigma_i, \quad (3)$$

the proposed ground state can be seen to exhibit a charge-stripe pattern [see Fig. 2 (b)].

Here we confirm the proposed low temperature ordered state and study in detail the thermodynamic behaviour of the system, by devising an appropriate order parameter and performing extensive Monte Carlo simulations that manage to achieve thermodynamic equilibrium below the ordering temperature.

Upon inspecting the spin configuration in Fig. 2 (a), we notice that one sublattice of the kagome triangles (in this instance, sublattice 1) is completely polarised, with the state having zero magnetisation overall. This observation leads us to postulate that the proposed ground state, which breaks time-reversal and sublattice symmetries, can be described by an appropriate order parameter

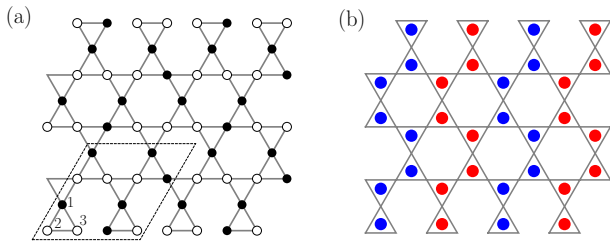


FIG. 2. Proposed ground state of the dipolar kagome Ising antiferromagnet. (a) The spins exhibit a pattern which breaks both time-reversal and sublattice symmetries, with one sublattice polarised (here, sublattice 1). The 12-site magnetic unit cell is outlined (rhomboid box). Black points indicate ‘up’ spins ($\sigma = 1$) and white points ‘down’ spins ($\sigma = -1$). (b) The charges Q (defined in the text) exhibit a charge-stripe pattern: red dots indicate positive charges ($Q = 1$) and blue dots negative charges ($Q = -1$).

for the transition, namely, the sublattice magnetisation

$$m_a = \frac{3}{N} \sum_{i \in \text{sublat. } a} \sigma_i, \quad (4)$$

where $a \in \{1, 2, 3\}$. The proposed ground state has one sublattice $a \equiv a'$ polarised such that $m_{a'} = \pm 1$, and the other two sublattices with $\sum_{a \neq a'} m_a = \mp 1$, such that the state has zero magnetisation overall. Notice the spin pattern on the two non-polarised sublattices: it has period four, with three spins $\sigma = \mp 1$ followed by one spin $\sigma = \pm 1$ [along the horizontal bonds in Fig. 2 (a)]; such lines of spins are stacked in a specific chiral structure.

To verify this, we performed extensive Monte Carlo (MC) simulations of the DKIAFM Hamiltonian (1) using a 12-site unit cell commensurate with the proposed ground state. Our system contains $N = 12L^2$ spins. To ensure that we do not exclude other possible ordered states, we also considered system sizes that are commensurate with plausible competing phases, which include the $\sqrt{3} \times \sqrt{3}$ state¹⁹. Unlike Chioar *et al.* (see Refs. 5 and 20), we sum the pairwise dipolar interactions via the method of summation of copies employed in Refs. 16 and 21, until convergence of one part in 10^6 . Since loop dynamics do not appear to help in alleviating the freezing⁵, we use Metropolis single spin-flip dynamics throughout. We cool the system from equilibrium at $T/D = 1$ in increments of $0.5 \times 10^{-3} D$, using 2×10^4 modified MC sweeps²² for equilibration at each temperature step. We time-average at each temperature by measuring quantities 400 times, each measurement separated by 50 modified MC sweeps, and we ensemble-average the results over 64 independent simulations. We note that this simulation protocol requires a substantial investment of computational resources but, by careful analysis of spin autocorrelation functions, we are able to ensure thermodynamic equilibrium down to temperatures lower than the transition temperature, at least for sufficiently small system sizes as discussed below.

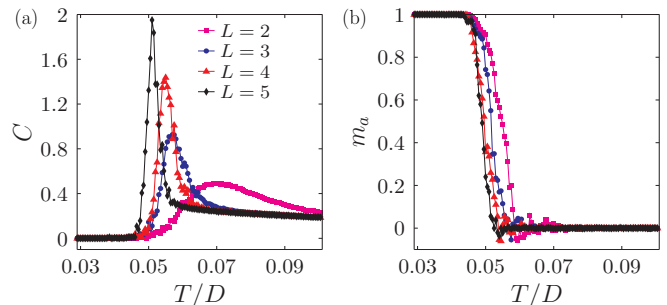


FIG. 3. (a) Heat capacity C and (b) sublattice magnetisation m_a of the DKIAFM for system sizes $L = \{2, 3, 4, 5\}$. The ordering transition to the proposed ground state is signalled by a peak in the heat capacity C and concomitant increase in the sublattice magnetisation m_a which acts as an order parameter.

The heat capacity C and sublattice magnetisation m_a are shown in Fig. 3 (a) and (b) respectively, for system sizes $L = \{2, 3, 4, 5\}$, with $N = \{48, 108, 192, 300\}$ spins. The ordering transition is signalled by a peak in the heat capacity (at around $T_c/D \simeq 0.05$ for $L = 5$), and a clear concomitant increase in m_a from zero to one, signalling the complete development of order consistent with the proposed ground state. Direct inspection of the spin configurations confirms that indeed the system in each case reaches the proposed ground state. The freezing of spin dynamics at low temperatures is remarkably strong, and we were unable to fully equilibrate systems larger than $L = 5$ (300 spins).

As shown in Fig. 3 (b), the order parameter m_a presents a jump which becomes increasingly sharp for larger system sizes. This trend towards discontinuous behaviour (rather than power-law behaviour) is suggestive of a first-order phase transition. The average energy per spin $\langle e \rangle$, which can be seen in the inset of Fig. 4, also displays an abrupt decrease at the transition temperature, the sharpness of which increases for larger systems²³. This is consistent with the latent heat expected to accompany a first-order transition.

The associated energy histogram $p(e)$ is shown in Fig. 4, at temperatures just above ($T/D = 0.060$), approximately at ($T/D = 0.052$), and just below ($T = 0.0505$) the transition (for $L = 5$). Above the transition, there is a single Gaussian-like peak which indicates a unique phase. The emergence close to the transition temperature of a double-peaked structure indicates the coexistence of two distinct phases of different energies (one of which is the ground state), and thus a first-order transition. At lower temperatures, the higher-energy peak disappears as the system increasingly occupies the ground state.

We have examined the scaling of the maximum of the heat capacity peak C_{\max} with the system size L , but do not find convincing evidence for it scaling with the volume of the system ($\propto L^2$), as expected for a first-order transition (not shown). Possible deviations could

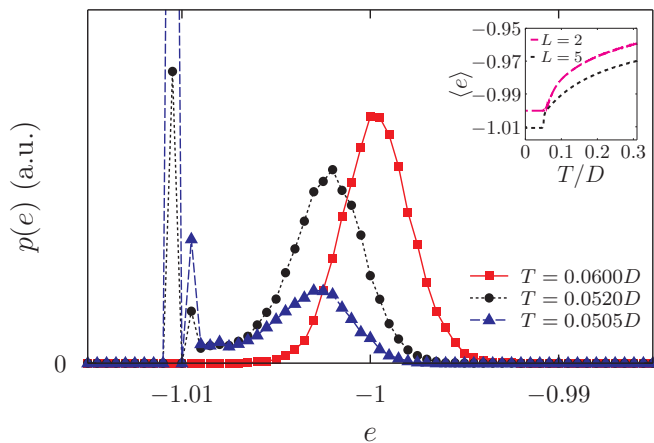


FIG. 4. Energy histogram $p(e)$ around the transition temperature for $L = 5$ (the largest system size we are able to fully equilibrate). Just above the transition temperature ($T/D = 0.06$), a single Gaussian-like peak indicates the presence of a unique phase. Around the transition temperature ($T/D = 0.052$), $p(e)$ displays a double-peaked structure indicating the coexistence of two distinct phases (one of which is the ground state), and thus a first-order transition. At lower temperatures ($T/D = 0.0505$), the higher-energy peak becomes comparatively much less pronounced as the system increasingly occupies the low-energy state. Inset: average energy per spin $\langle e \rangle$ as a function of temperature T for two different system sizes $L = 2, 5$. The transition is signalled by an abrupt decrease in the energy $\langle e \rangle$, the sharpness of which increases with system size.

be due to strong finite-size effects for the modest system sizes that we are able to equilibrate reliably. Similar behaviour has been found in studies of first-order transitions in long-range interacting Ising spin systems on the square lattice²⁴.

IV. SPIN RELAXATION AT LOW TEMPERATURES

At very low temperatures the DKIAFM exhibits a stupendous freezing of its spin dynamics, which we study quantitatively using the spin autocorrelation function

$$C(t) = \frac{1}{N} \sum_i \sigma_i(0) \sigma_i(t). \quad (5)$$

We consider single spin-flip dynamics and we focus on the behaviour of the autocorrelation function in thermodynamic equilibrium, equivalent to the $t_w \rightarrow \infty$ limit of the two-time autocorrelation function $C(t, t_w)$. The decay of $C(t)$ is not captured by a simple exponential, but is rather described by a stretched exponential,

$$C(t) = \exp[-(t/\tau)^\beta], \quad (6)$$

where τ is the relaxation timescale and $\beta \leq 1$ is the Kohlrausch exponent. Stretched-exponential relaxation

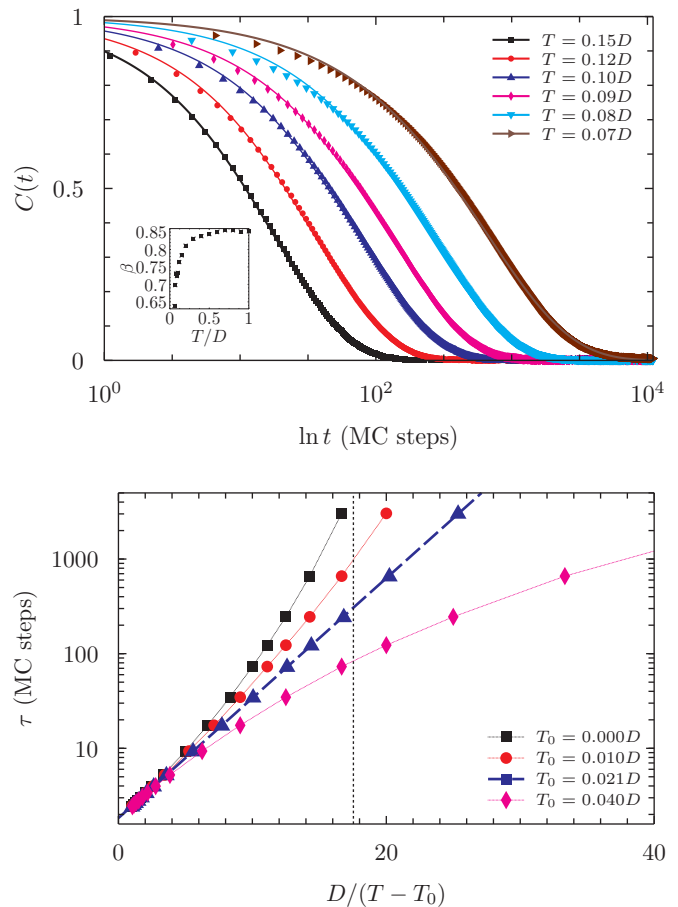


FIG. 5. Top: examples of spin autocorrelation functions (symbols) and relative stretched exponential fits (solid lines), used to extract τ and β . The behaviour of the latter as a function of temperature is shown in the inset. The system size is $L = 3$. Bottom: spin autocorrelation time τ as a function of inverse temperature (black squares) in semilogarithmic scale. The noticeable departure from linear scaling at low temperatures is characteristic of super-Arrhenius behaviour. The vertical line indicates the finite-size transition temperature $T_c/D \simeq 0.057$. The same data are also plotted against $D/(T - T_0)$ to show that τ diverges according to a Vogel-Fulcher form with $T_0/D \simeq 0.0235$ and $\Delta/D \simeq 0.27$ (the dashed blue line is the corresponding fit to the data).

is typical of systems with complex energy landscapes and often associated with glassy or supercooled liquid behaviour²⁵. We fit a stretched exponential to $C(t)$ and extract both the relaxation time τ and stretching exponent β for different temperatures T (see e.g., the top panel of Fig. 5)²⁶.

The relaxation time τ for an $L = 3$ system obtained from the fit to $C(t)$ is plotted as a function of inverse temperature T (in units of D) in the bottom panel of Fig. 5. The approximate finite-size transition temperature for the $L = 3$ system, $T_c/D = 0.057 \pm 0.002$, is indicated by the vertical line. There is clear evidence of super-Arrhenius behaviour as the temperature is lowered (above T_c). The stretching exponent β as a func-

tion of temperature is shown in the inset of Fig. 5 (top), demonstrating that the decay of $C(t)$ becomes increasingly stretched at low temperatures.

In the bottom panel of Fig. 5 we also plot the timescale τ on a logarithmic scale as function of $D/(T - T_0)$ for different values of T_0 , in order to examine the super-Arrhenius behaviour. Thanks to the two-dimensional nature of the system, we were able to push the numerical simulations to access long times and explore a reasonably large range of relaxation time scales. As a result, we find good evidence that the timescales obey a Vogel-Fulcher form

$$\tau \sim \exp\left(\frac{\Delta}{T - T_0}\right), \quad (7)$$

with $T_0/D = 0.020 \pm 0.003$ and $\Delta/D = 0.28 \pm 0.02$. Note the very long relaxation times ($\tau \sim 10^5$ MC steps per spin) at the lowest temperatures. This Vogel-Fulcher form for the relaxation time τ is again characteristic of fragile glass behaviour in the system²⁵, which goes hand-in-hand with the supercooled behaviour that we observe.

V. BEHAVIOUR OUT OF EQUILIBRIUM

We also ran simulations with larger systems, of size $L \in \{9, 12, 15\}$, the features of which we discuss briefly here in regard to out of equilibrium behaviour. For these system sizes, the cooling protocol described above is not sufficient to thermalise the system. However, the slower the cooling protocol, the more pronounced the peak in the heat capacity signalling the incipient transition becomes. The developing order is more prominently visible in the behaviour of the order parameter that we identified in this work (see Sec. III). Even though the value of the order parameter remains far smaller than the saturated value at all temperatures, it becomes distinctly non-zero – well above statistical fluctuations – at a well-defined temperature that we identify as a reasonable proxy for the thermodynamic transition temperature T_c of the system [see Fig. 6 (b)].

Understanding the onset of the ordered phase below T_c when the system is out of equilibrium is hindered by the elaborate spin pattern of the 12-site magnetic unit cell. We can gain some visual intuition by taking advantage of the fact that one of the sublattices is fully polarised in the ordered state. In Fig. 7, we plot separately the individual sublattices $a = \{1, 2, 3\}$ of a low-temperature spin configuration in an $L = 9$ system. Each sublattice forms a triangular lattice. A system which is fully ordered in the ground state would have one sublattice fully polarised (say, all black), and the two other sublattices partially polarised in the opposite direction (say, mostly white) – with a pattern where one row is fully polarised and the next row has alternating sign. This behaviour can indeed be recognised in some regions of the system in Fig. 7 (for example, the white top-right region for $a = 1$ and corresponding regions for the other sublattices). By

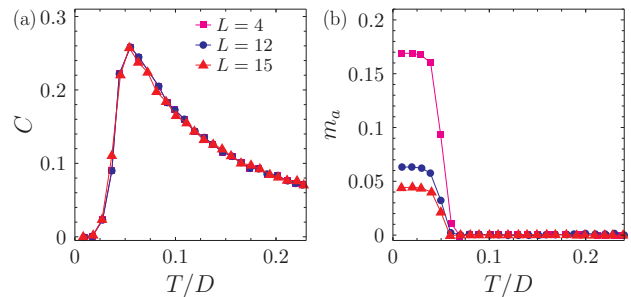


FIG. 6. Behaviour of (a) the heat capacity C and (b) the sublattice magnetisation m_a for systems sizes $L = \{4, 12, 15\}$ as a function of temperature T in the case where the number of sweeps per temperature step is insufficient to equilibrate the system.

examining individual sublattices in this way, it is clear that the system exhibits some domains consistent with the ground-state order, although identifying boundaries between domains is difficult.

In the right panel of Fig. 7, we plot the corresponding configuration of the charges Q . In the charge picture, it is not immediately easy to identify ordered domains, but on more detailed inspection one can recognise patches of parallel charge stripes, reminiscent of the charge order of the ground state [see Fig. 2 (b)]. The different domains, with charge stripes oriented along different lattice directions, compete with one another, leading to a dendritic arrangement of charge stripes. The charge configuration corresponds thus to a kind of ‘stripe liquid’, similar to that observed in a study by Mahmoudian and coworkers³ of frustrated Coulomb liquids on the triangular lattice at half filling. In that work, the authors also observe slow dynamics due to a large manifold of low-lying metastable states; however the divergence of the relaxation timescales at low temperatures in that system is of the more common Arrhenius behaviour, characteristic of strong rather than fragile glasses. Patches with packed parallel stripes of charges require coordinated ‘topological’ (system-spanning) rearrangements of the spin orientations in order to move between low energy states. It is tantalising to speculate that an appropriate effective modelling of such spin rearrangements may be key to understanding the slow dynamics in these systems (see Appendix B).

VI. DISCUSSION AND CONCLUSIONS

To summarise, we have investigated the nature of the ordered phase and phase transition in the dipolar kagome Ising antiferromagnet (DKIAFM). By means of extensive Monte Carlo simulations, and the identification of a suitable order parameter, we were able to confirm the ground state proposed in Ref. 5. We also provided evidence that the transition is first order.

Interestingly, we notice that a Coulombic system of

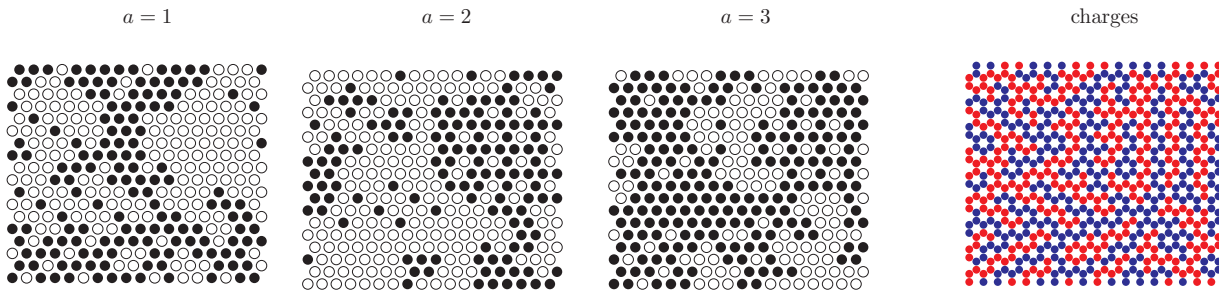


FIG. 7. Individual sublattices $a = \{1, 2, 3\}$ of a low-temperature spin configuration in an $L = 9$ system are plotted separately in the first three panels from the left. Each sublattice constitutes a triangular lattice. Regions of full polarisation in one sublattice can clearly be seen (for example, the white top-right region for $a = 1$), with the corresponding regions in the other sublattices polarised mostly in the opposite direction (mostly black). Note the typical pattern of the partially polarised sublattices, with rows of spins that alternate between fully-polarised and alternating sign. The values for the overall sublattice magnetisations of this configuration are $m_1 = -0.074$, $m_2 = -0.185$, and $m_3 = 0.259$. The corresponding charge configuration is shown in the right panel, exhibiting a characteristic dendritic stripe pattern.

charges hopping on a kagome lattice⁴ appears to exhibit a remarkably similar ordering tendency to the present system, which is also prevented by slow dynamics. We wonder whether the hitherto puzzling ordered state underpinning Fig. 1 in Ref. 4 may indeed be the same ordered state demonstrated in our work. It may indeed be possible to establish an intuitive connection between the orders exhibited by the two models via the charge mapping discussed in Appendix B.

Upon approaching the phase transition, the DKIAFM exhibits a remarkable propensity to fall out of equilibrium and enter a supercooled liquid phase, avoiding any sign of the full transition altogether⁵. We studied the equilibrium behaviour of the spin autocorrelation function above the transition, and observed that it is well described by a stretched exponential form, typical of glass-forming systems. From the stretched exponential relaxation we obtained the temperature dependence of the equilibrium relaxation time scale and found it to obey a Vogel-Fulcher law, typical of fragile glasses.

This is a remarkable result in a system without disorder with an eminently simple two-body Hamiltonian, in the absence of dynamical constraints (single spin flip updates). The behaviour cannot be related – to the best of our understanding – to the avoided criticality paradigm: the short range interaction terms in the Hamiltonian are frustrated and do not lead per se to a continuous phase transition; moreover, dipolar interactions are not sufficiently long-ranged to suppress an ordering transition irrespectively of their strength.

Our work propels the DKIAFM to the fore in the study of glassy dynamics in systems without disorder. Further work is needed to understand the origin of the dynamical slowing down – here we merely conjecture that it may be related to topological spin rearrangements between low-lying energy states, via an effective dumbbell and charge description (discussed in Appendix B). What makes this system even more interesting is the potential of experimental verification in several realistic set ups,

from colloidal crystals, to artificial nanomagnetic arrays, to (layered) bulk kagome materials.

Appendix A: Quantifying frustration

In the following we study the level of frustration present in the DKIAFM by considering Pauling estimates of the ground state degeneracy as the range of the interactions is progressively increased. This illustrates how ordering in the model is expected to arise only from (some) third neighbour or longer-ranged terms. We also compute the Fourier transform of the full interaction matrix, showing a lowest band that is substantially flatter than the full spectrum bandwidth: another hallmark of a highly frustrated system.

1. Pauling estimates for truncated interactions

We consider here the Hamiltonian (1) truncated at third neighbour distance, and written for convenience as

$$\mathcal{H} = J_1 \sum_{\langle ij \rangle} \sigma_i \sigma_j + J_2 \sum_{\langle\langle ij \rangle\rangle} \sigma_i \sigma_j + J_3 \sum_{\langle\langle\langle ij \rangle\rangle\rangle} \sigma_i \sigma_j. \quad (\text{A1})$$

In accordance with the choice of parameters in Sec. II, we set $J_1 = 1.5$, $J_2 \simeq 0.692$, and $J_3 = 0.625$. The second and third neighbour distances on the kagome lattice are illustrated for convenience in Fig. 8. Notice that there are two types of third neighbour distances, whose length is exactly twice the kagome lattice constant: one type is across the hexagonal cells, and the other is along two aligned consecutive bonds (not shown). The J_3 term in Eq. (A1) encompasses both types.

A simple Pauling argument allows to estimate the ground-state degeneracy of the J_1 - J_2 - J_3 model in various regimes. For $J_2 = J_3 = 0$, the model reduces to the nearest-neighbour kagome spin ice model of Wills, Ballo and Lacroix²⁷, for which a Pauling estimate gives an

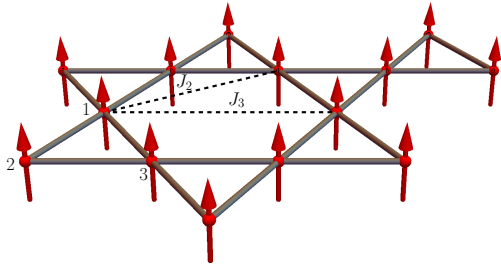


FIG. 8. Illustration of second (J_2) and third (J_3) neighbour interaction distances on the kagome lattice, indicated by the dashed lines.

entropy of $\ln[2(3/4)^{2/3}] \simeq 0.5014$ per spin (this is very close to the known exact value 0.5018^{28}).

The J_2 interactions form three independent kagome superlattices on which they try to enforce the ice rules (the triangles of these superlattices live inside the hexagons of the original lattice). Each kagome superlattice has $N'_{\text{tri}} = N_{\text{tri}}/3$ triangles, where $N_{\text{tri}} = 2N_s/3$ is the number of triangles in the original kagome lattice (N_s being the total number of spins). Therefore the number of possible states can be estimated starting from the nearest-neighbour J_1 result as

$$\begin{aligned}
 \Omega &\simeq \underbrace{2^{N_s} \times \left(\frac{6}{8}\right)^{N_{\text{tri}}}}_{\text{kagome ice rule result}} \\
 &\times \underbrace{\left(\frac{6}{8}\right)^{N'_{\text{tri}}} \times \left(\frac{6}{8}\right)^{N'_{\text{tri}}} \times \left(\frac{6}{8}\right)^{N'_{\text{tri}}}}_{\text{constraint from three kagome superlattices}} \\
 &= 2^{N_s} \times \left(\frac{6}{8}\right)^{2N_{\text{tri}}} = 2^{N_s} \times \left(\frac{6}{8}\right)^{4N_s/3} \\
 &\simeq (1.363)^{N_s}. \tag{A2}
 \end{aligned}$$

This leads to an entropy $\mathcal{S}_{J_1-J_2} = \ln \Omega \simeq 0.309N_s$.

Similarly, the J_3 interactions form three triangular superlattices on which they try to enforce the ice rules (these are simply the three sublattices of the original kagome lattice). Each triangular superlattice has $N''_s = N_s/3$ spins and thus $N''_{\text{tri}} = 2N''_s = 2N_s/3 = N_{\text{tri}}$ triangles. Therefore the number of possible states can be

estimated starting with the J_1 - J_2 result as

$$\begin{aligned}
 \Omega &\simeq \underbrace{2^{N_s} \times \left(\frac{6}{8}\right)^{2N_{\text{tri}}}}_{J_1-J_2 \text{ interactions}} \\
 &\times \underbrace{\left[\left(\frac{6}{8}\right)^{N''_{\text{tri}}}\right]^3}_{\text{constraint from three triangular superlattices}} \\
 &= 2^{N_s} \times \left(\frac{6}{8}\right)^{10N_s/3} \\
 &\simeq (0.767)^{N_s}. \tag{A3}
 \end{aligned}$$

This leads to an entropy $\mathcal{S}_{J_1-J_2-J_3} = \ln \Omega \simeq -0.266N_s$, which is negative and suggests that the system orders. (Alternatively, one could use the known residual entropy per spin of a triangular Ising antiferromagnet, $\mathcal{S}_{\text{TIAFM}} = 0.32306$, to estimate a Pauling-like reduction factor for each of the three triangular superlattices of $(0.691)^{N''_s}$. Substituting this term inside the square bracket in the second line of Eq. (A3), one obtains $\Omega \simeq (0.94)^{N_s}$ and $\mathcal{S}_{J_1-J_2-J_3} \simeq -0.06N_s$, which is still negative but only very marginally so.)

It is interesting to notice that, if only a subset of the third-neighbour (J_3) interactions are kept (those across the hexagons as illustrated in Figure 1, but not those along the bonds of the lattice), and if we set $J_1 = J_2 = J_3$, then the effective model is one where the energy can be written in terms of a sum over all hexagons of the squared magnetisation of each hexagon. The ground states of this model have zero total magnetisation on each hexagon and a Pauling estimate suggests a residual ground state degeneracy of $\mathcal{S}_{\text{hex}} = (N_s/3) \ln(5/2) \simeq 0.305N_s$ (20 out of the 64 possible spin arrangements on a hexagon have null magnetisation, and there are $N_s/3$ hexagons in a kagome lattice of N_s spins). This is an interesting model which might warrant further investigation in the future.

2. Simulations

We investigate the above predictions with Monte Carlo simulations of the J_1 - J_2 - J_3 Hamiltonian (A1).

Figure 9 shows the results for the heat capacity per spin C and entropy S for the J_1 only case (a), the J_1 - J_2 case (b), and the J_1 - J_2 - J_3 case (c), for a system of size $L = 3$. As mentioned above, the J_1 only case is equivalent to the nearest-neighbour kagome ice model of Wills, Ballou, and Lacroix²⁷, and correspondingly displays a broad Schottky peak in the heat capacity C at around $T \sim 2$ (in units where $J_1 = 1.5$) signalling the onset of the kagome ice rules, and a drop in the entropy S down to a value in good agreement with the Pauling estimate of 0.501 per spin (dashed line).

The J_1 - J_2 case displays an additional bump in the heat capacity at a slightly lower temperature around $T \sim 0.5$,

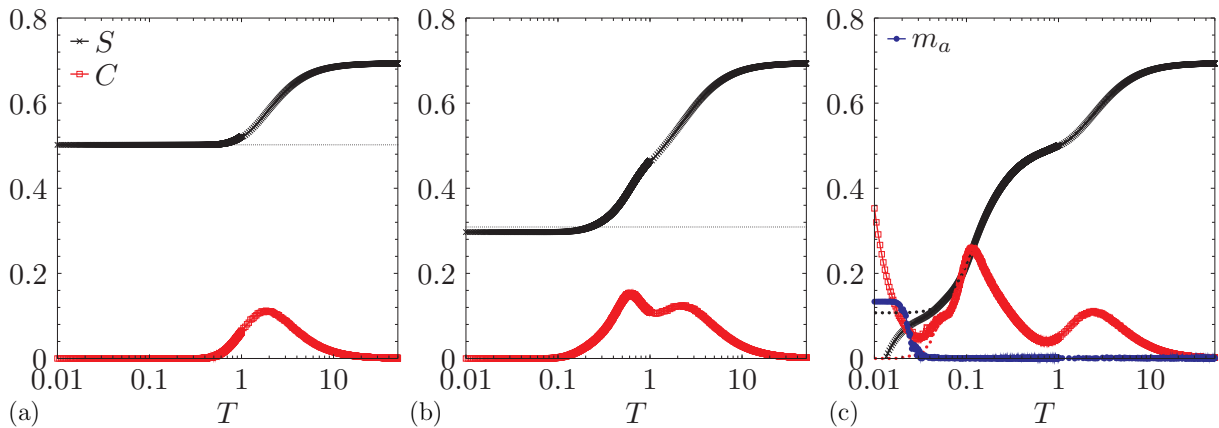


FIG. 9. Heat capacity per spin C and entropy S of the effective J_1 - J_2 - J_3 model (plotted on the same axis). (a) J_1 only. This model is equivalent to the nearest-neighbour kagome spin ice model. It exhibits a ground-state entropy in good agreement with the Pauling estimate of 0.501 per spin (dashed line). (b) J_1 - J_2 . This model exhibits a second peak in the heat capacity at lower temperatures, associated with the onset of the ice rules on the kagome superlattices dictated by the J_2 interactions. The ground-state entropy is in good agreement with the Pauling estimate of 0.309 per spin (dashed line). (c) J_1 - J_2 - J_3 . After the second feature in the heat capacity, the model falls out of equilibrium, as indicated by the difference between the ensemble-averaged results (points) and time-averaged results (dashed line) for the heat capacity and the spin entropy. Also plotted is the sublattice order parameter m_a , which displays an increase from zero, hinting at ordering consistent with the dipolar ground state. The system size is $L = 3$ and the coupling constants, where not vanishing, are $J_1 = 1.5$, $J_2 \simeq 0.692$, and $J_3 = 0.625$.

and a drop in the entropy to a value close to the Pauling estimate of 0.309 per spin (dashed line). We therefore ascribe the lower-temperature feature in the heat capacity to the onset of the ice rules on the three kagome superlattices.

In the J_1 - J_2 - J_3 case, after the onset of the kagome ice rules, the second feature in the heat capacity is pushed to lower temperatures, and the system falls out of equilibrium, signalled by the difference between the ensemble-averaged results, and the purely time-averaged results. The divergence of the heat capacity at low temperatures in the ensemble-averaged case indicates that the system does not find a unique energy minimum, despite us using extremely slow annealing protocols at low temperatures, as in the study of the full dipolar case above (for concreteness, we cool from $T = 1$ in decrements of 5×10^{-4} using 2×10^4 modified MC sweeps for equilibration at each temperature step).

Despite our inability to equilibrate the system, we do find a small signature of a trend towards the proposed ground state. The order parameter m_a from Eq. (4) remains zero up to fluctuations for the J_1 - J_2 case at all temperatures, whereas for the J_1 - J_2 - J_3 case it increases from zero to a value of about 0.13 for temperatures lower than approximately $T = 0.03$, signalling some development of order consistent with the proposed ground state [see Fig. 9 (c)]. However, other types of order are consistent with this signature, and further work is needed to say anything conclusive on the matter. It seems that the J_1 - J_2 - J_3 model is perhaps even more frustrated than the full dipolar model, and that further-neighbour interactions play a key role in relieving some frustration and selecting the ground state.

3. Interaction matrix

Each lattice site $i \equiv (l, a)$ has an index l which labels the sites of the Bravais lattice formed by the centres of the up-type kagome triangles, and an index $a \in \{1, 2, 3\}$ which labels the sublattice (see Fig. 1). Namely, the spins $\mathbf{S}_i \equiv \mathbf{S}_l^a \equiv \mu \sigma_l^a \hat{\mathbf{e}}_z$ have positions $\mathbf{r}_i \equiv \mathbf{r}_l^a \equiv \mathbf{R}_l + \mathbf{e}^a$, where $\{\mathbf{R}_l\}$ point to the centres of the up triangles, and $\{\mathbf{e}^a\}$ are the vectors from the centres of the triangles to each of the three spins,

$$\mathbf{e}^1 = (0, 1/\sqrt{3}) \quad (\text{A4})$$

$$\mathbf{e}^2 = (-1, -1/\sqrt{3})/2 \quad (\text{A5})$$

$$\mathbf{e}^3 = (1, -1/\sqrt{3})/2, \quad (\text{A6})$$

in units of the kagome lattice constant.

The Hamiltonian (1) can then be written as

$$\mathcal{H} = \sum_{lm} \sum_{ab} J^{ab}(\mathbf{R}_{lm}) \sigma_l^a \sigma_m^b, \quad (\text{A7})$$

where $\mathbf{R}_{lm} \equiv \mathbf{R}_m - \mathbf{R}_l$. In Fourier space,

$$\mathcal{H} = \sum_{\mathbf{q}} \sum_{ab} J^{ab}(\mathbf{q}) \sigma_{\mathbf{q}}^a \sigma_{-\mathbf{q}}^b, \quad (\text{A8})$$

where $\sigma_l^a = \sum_{\mathbf{q}} \sigma_{\mathbf{q}}^a \exp(i\mathbf{q} \cdot \mathbf{r}_l^a)$, and

$$J^{ab}(\mathbf{R}_{lm}) = \sum_{\mathbf{q}} J^{ab}(\mathbf{q}) \exp(i\mathbf{q} \cdot \mathbf{r}_{lm}^{ab}), \quad (\text{A9})$$

is the 3×3 interaction matrix, where $\mathbf{r}_{lm}^{ab} \equiv \mathbf{r}_m^b - \mathbf{r}_l^a$.

The eigenvalue spectrum $\lambda^n(\mathbf{q})$ of $J^{ab}(\mathbf{q})$ is shown in Fig. 10. It has three branches due to the three sites in

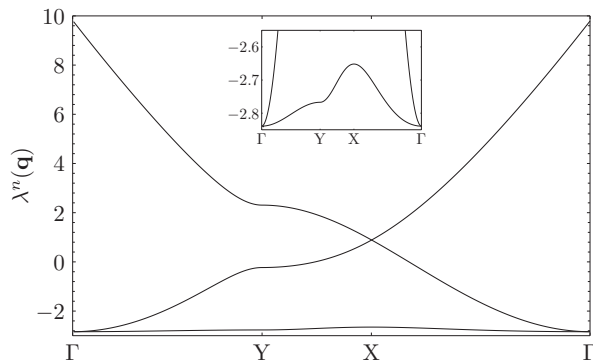


FIG. 10. Eigenvalues $\lambda^n(\mathbf{q})$ of the Fourier transform of the interaction matrix $J^{ab}(\mathbf{q})$ on a path in the Brillouin zone, $\Gamma \rightarrow Y \rightarrow X \rightarrow \Gamma$. There are three branches due to the three sites in the unit cell. The flatness of the bottom branch is characteristic of frustration. Inset: zoom on the bottom branch $\lambda^{\min}(\mathbf{q})$, which presents a minimum at the Γ point.

the unit cell. The flatness of the bottom branch $\lambda^{\min}(\mathbf{q})$ (illustrated in detail in the inset of Fig. 10) is characteristic of frustration in the model. Notice that its bandwidth is only about 2% of that of the full spectrum. The minimum at the Γ point suggests that, at mean-field level, the leading ordering instability from the high-temperature phase is expected to be at $\mathbf{q}^* = (0,0)$. (Our results are the extension to the Ising case of the results found for Heisenberg spins by Maksymenko and coworkers²⁹).

Appendix B: Effective charge picture, emergent charge stripes and freezing

To better understand the nature of the low energy states in the DKIAFM, it is interesting to draw a parallel with a related model: kagome ice²⁷. In the latter, the Ising spins lie within the plane of the lattice, and point directly into or out of a triangle. A useful way of understanding kagome ice derives from the so-called dumbbell picture, where each spin is represented as a pair of magnetic charges $\pm q$ separated by a distance a , such that $\mu = qa$ ^{30,31}. Specifically, it is customary to choose a so that the three charges in each triangle of the kagome lattice meet precisely at its centre. To leading order, the Hamiltonian of kagome ice can then be written in terms of the total charges Q_α inside each triangle (labelled by α),

$$\mathcal{H}_{\text{eff}} = \sum_{\alpha} \frac{1}{2} v_0 Q_{\alpha}^2 + \frac{\mu_0}{8\pi} \sum_{\beta < \alpha} \frac{Q_{\alpha} Q_{\beta}}{r_{\alpha\beta}}. \quad (\text{B1})$$

The first term is a chemical potential of strength v_0 for the charges, and the second term is a long-range Coulomb interaction between them. Notice that the lattice formed by the centres of the triangles is a honeycomb lattice dual to the original kagome lattice. Much of the physics of kagome ice can be understood more intuitively in terms

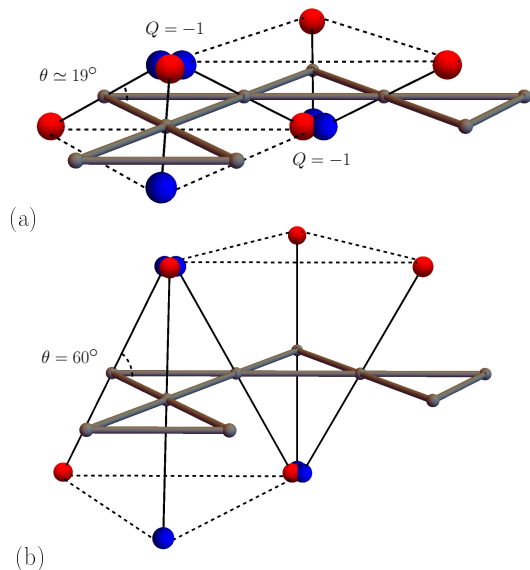


FIG. 11. Each spin of magnitude μ is decomposed into a dumbbell, i.e., a pair of charges of strength $\pm q$ separated by a distance a such that $\mu = qa$. Starting in-plane charges, with the distance a chosen so that the charges at the end of the dumbbells overlap at the centres of the triangles, we progressively tilt the spins out of the plane of the lattice. In the process, we increase a and correspondingly reduce q so that the charges remain overlapping and $\mu = qa$ is kept constant. The sum of three overlapping charges is proportional to the corresponding triangular charge Q_α introduced in the main text (and shown as Q in the figure). The limiting case of spins perpendicular to the kagome plane corresponds to the DKIAFM, which can then be seen as two infinitely separated triangular layers of charges (indicated by the dashed lines).

of such system of interacting charges than in terms of the original spins.

Inspired by the dumbbell construction of the charges in kagome ice, one can view the DKIAFM as the limit where the spins are progressively tilted until they become perpendicular to the kagome plane (as illustrated pictorially in Fig. 11). In the process, one ought to take the limit $a \rightarrow \infty$ (and, correspondingly, $q \rightarrow 0$) to preserve the charges at the end of the dumbbells overlapping at the same location. (Notice that the magnetic charges Q_α associated with each triangle in the dumbbell picture are in fact proportional to the charges $Q_\Delta = \sum_{i \in \Delta} \sigma_i$ and $Q_\nabla = -\sum_{i \in \nabla} \sigma_i$ introduced in Sec. III.)

Of course, the greater the tilt the less accurate the dumbbell picture becomes, and at some point the description in terms of resummed charges ought to break down. However, we are tempted to ignore this issue and see what the naive limiting scenario suggests about the behaviour of the system. Resumming the charges as above leads to a description in terms of two triangular layers (one formed by the centres of the up kagome triangles; the other by the centres of the down kagome tri-

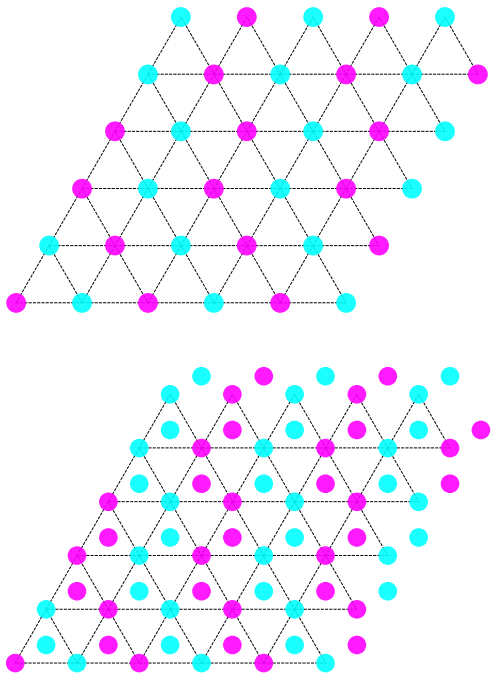


FIG. 12. Coulomb-interacting positive (magenta) and negative (cyan) charges on the triangular lattice are expected to order in patterns like that in the top panel, with charges alternating along one lattice direction and random along the other. Notice that one can view the charge pattern in terms of stripes along the lattice bonds (running largely from top to bottom in the configuration chosen here). The interactions between the two layers, dictated by the dipolar coupling between the underlying spins, favours like charges close to one another across layers, and leads to an overall charge arrangement like the one in the bottom panel, also exhibiting charge stripes. There is a whole class of these energetically low-lying states, which includes the dipolar ground state.

angles, shown as dashed lines in Fig. 11) that, to first approximation, are decoupled from one another. The coupling within each triangular layer is due to the (antiferromagnetic) Coulomb interaction between charges given by the second term in the effective Hamiltonian (B1). Such a Coulomb-interacting system on the triangular lattice is predicted^{32,33} to be partially frustrated and have ground states where charges alternate in one lattice direction, but are random in the other direction. An example is illustrated in Fig. 12 (top panel). These states can be viewed as charge-stripe patterns on the triangular lattice, with alternating lines of like charges that correspond to

the path of a random walk that can either turn left or right as it moves vertically from one row to the next. There is a whole family of $\sim 2^L$ such states, each corresponding to a particular choice of path for the stripes.

The two triangular layers appear decoupled in terms of the Coulomb interaction between the resummed charges Q_α , which in the limit of dumbbells perpendicular to the plane are infinitely separated from one another. However, the dipolar interaction between the original spins can be seen to favour like-charges to sit close to one another across layers. Indeed, a charge in one layer adjacent to a charge of the same sign in the other layer corresponds to a mainly antiferromagnetic (and thus energetically favoured) spin arrangement, as illustrated in Fig. 11 (b). If we pair the top and bottom triangular charge layers, each in one of their stripe configurations, so as to maximise the proximity between like charges across layers, we obtain overall charge arrangements like the one illustrated in Fig. 12 (bottom panel). One triangular layer becomes slave to the other, but a $\sim 2^L$ degeneracy survives and it again takes the form of charge stripes randomly turning left and right as they stretch across the lattice. The total number of states in this family is thus sub-extensive, i.e., its entropy scales with the linear size of the system. Remarkably, one of these states is indeed the 7 shape ground state of the DKIAFM, illustrated in Fig. 2, (b).

Whereas we have clearly taken the dumbbell picture and corresponding charge representation well beyond its limit of validity, and the energetic arguments above cannot be trusted per se, one can compute the actual energies of various charge-stripe configurations such as that in Fig. 12 (bottom panel) in terms of original spins via the Hamiltonian (1). We find that many of them lie very close in energy to the ground state (with an energy difference of as little as 1.3%), whilst differing from it in configuration space by a topological rearrangement of at least $\mathcal{O}(L)$ spins. Indeed, in order to change a charge stripe state into another without introducing costly defects (dislocations, namely stripe end-points and branching), one needs to modify the spin configuration so as to ‘move’ the charge stripes consistently across the whole system, which amounts to an extensive number of (system-spanning) topological updates.

We conjecture that the existence of this sub-extensive manifold of energetically low-lying, but configurationally topologically distinct, states is one of the key reasons underpinning the exceptionally strong freezing observed in the DKIAFM at low temperatures.

* james.o.hamp@gmail.com

¹ G. Tarjus, S. A. Kivelson, Z. Nussinov, and P. Viot, *Journal of Physics: Condensed Matter* **17**, R1143 (2005).

² M. Dzero, J. Schmalian, and P. G. Wolynes, in *Structural Glasses and Supercooled Liquids: Theory, Experiment, and Applications*, edited by P. G. Wolynes and

V. Lubchenko (John Wiley & Sons, Inc., Hoboken, NJ, USA, 2012) Chap. 5, pp. 193–221.

³ S. Mahmoudian, L. Rademaker, A. Ralko, S. Fratini, and V. Dobrosavljevi, *Physical Review Letters* **115**, 025701 (2015).

⁴ T. Terao, *The European Physical Journal B* **89**, 209 (2016).

- ⁵ I. A. Chioar, N. Rougemaille, and B. Canals, *Phys. Rev. B* **93**, 214410 (2016).
- ⁶ Fragile glass behaviour in higher dimensional systems in the presence of long range interactions has been uncovered, in Refs. ? ? for example. However, the computational challenge of accessing large time scales prevented the authors from being able to analyse the super-Arrhenius temperature regime – a task that is just within reach in two dimensional systems.
- ⁷ F. Ritort and P. Sollich, *Advances in Physics* **52**, 219 (2003).
- ⁸ Y. Han, Y. Shokef, A. M. Alsayed, P. Yunker, T. C. Lubensky, and A. G. Yodh, *Nature* **456**, 898 (2008).
- ⁹ D. Zhou, F. Wang, B. Li, X. Lou, and Y. Han, *Physical Review X* **7**, 021030 (2017).
- ¹⁰ C. Nisoli, R. Moessner, and P. Schiffer, *Reviews of Modern Physics* **85**, 1473 (2013).
- ¹¹ K.-K. Ni, S. Oospelkaus, M. H. G. de Miranda, A. Pe'er, B. Neyenhuis, J. J. Zirbel, S. Kotochigova, P. S. Julienne, D. S. Jin, and J. Ye, *Science* **322**, 231 (2008).
- ¹² A. Griesmaier, J. Werner, S. Hensler, J. Stuhler, and T. Pfau, *Phys. Rev. Lett.* **94**, 160401 (2005).
- ¹³ A. Scheie, M. Sanders, J. Krizan, Y. Qiu, R. J. Cava, and C. Broholm, *Phys. Rev. B* **93**, 180407 (2016).
- ¹⁴ J. Paddison, H. Ong, J. Hamp, P. Mukherjee, X. Bai, M. Tucker, N. Butch, C. Castelnovo, M. Mourigal, and S. Dutton, *Nature Communications* **7**, 1 (2016).
- ¹⁵ Z. L. Dun, J. Trinh, M. Lee, E. S. Choi, K. Li, Y. F. Hu, Y. X. Wang, N. Blanc, A. P. Ramirez, and H. D. Zhou, *Phys. Rev. B* **95**, 104439 (2017).
- ¹⁶ G.-W. Chern, P. Mellado, and O. Tchernyshyov, *Phys. Rev. Lett.* **106**, 207202 (2011).
- ¹⁷ T. Takagi and M. Mekata, *J. Phys. Soc. Japan* **62**, 3943 (1993).
- ¹⁸ I. A. Chioar, N. Rougemaille, A. Grimm, O. Fruchart, E. Wagner, M. Hehn, D. Lacour, F. Montaigne, and B. Canals, *Phys. Rev. B* **90**, 064411 (2014).
- ¹⁹ The unit cell chosen for our system is not commensurate with all six proposed 7 shape ground states, given by the twofold time-reversal and threefold sublattice symmetries. Indeed, it is commensurate with only one of the three sublattices being fully polarised.
- ²⁰ I.-A. Chioar, *Artificial Kagome Spin Networks - From Short-Range Degeneracy towards Long-Range Dipolar Order*, Ph.D. thesis, Ecole normale supérieure de Lyon (2015).
- ²¹ G. Möller and R. Moessner, *Phys. Rev. B* **80**, 140409 (2009).
- ²² Following Ref. 5, we take a modified Monte Carlo sweep at a given temperature to correspond to $N \times r^{-1}$ single spin-flip attempts, where r is the acceptance ratio at that temperature. At the very lowest temperatures, the acceptance rate becomes extremely small ($r < 10^{-4}$), and it becomes unfeasible to adhere to this protocol. We therefore impose a cutoff, $r_{\text{cutoff}} = \max[r, 10^{-4}]$. We find that such a cutoff does not affect the ability of sufficiently small systems to order, and in fact it kicks in below the transition for the system sizes we treat here.
- ²³ Note that the difference in ground-state energies per spin for different system sizes is attributable to the different shapes of the boundary at infinity in the lattice summation of the dipolar energies.
- ²⁴ O. Osenda, F. A. Tamarit, and S. A. Cannas, *Phys. Rev. E* **80**, 021114 (2009).
- ²⁵ A. Cavagna, I. Giardina, and T. S. Grigera, *J. Chem. Phys.* **118**, 6974 (2003).
- ²⁶ We note that, for the very lowest temperature included in Fig. 5 (bottom), the proximity to the finite-size transition causes the autocorrelation function to saturate, $C(t) \rightarrow m^2 > 0$ for $t \gg 1$. Therefore, we fitted instead the connected autocorrelation function, $C(t) - m^2$.
- ²⁷ A. S. Wills, R. Ballou, and C. Lacroix, *Phys. Rev. B* **66**, 144407 (2002).
- ²⁸ K. Kanô and S. Naya, *Progress of Theoretical Physics* **10**, 158 (1953).
- ²⁹ M. Maksymenko, V. R. Chandra, and R. Moessner, *Phys. Rev. B* **91**, 184407 (2015).
- ³⁰ C. Castelnovo, R. Moessner, and S. L. Sondhi, *Nature* **451**, 42 (2008).
- ³¹ G.-W. Chern, P. Mellado, and O. Tchernyshyov, *Phys. Rev. Lett.* **106**, 207202 (2011).
- ³² J.-R. Lee and S. Teitel, *Phys. Rev. Lett.* **66**, 2100 (1991).
- ³³ J.-R. Lee and S. Teitel, *Phys. Rev. B* **46**, 3247 (1992).